CHAPTER V

INSTRUMENTAL TECHNIQUES

FOR PARTICLE SIZE DETERMINATION

5.1 INTRODUCTION

Particle size determination is very essential and important while working with nanomaterials. There are a few good experimental techniques, which are currently used by the researchers worldwide, for particle size determination. XRD, SEM, TEM, SPM, and particle size analyzers are some of the efficient and reliable techniques which can precisely determine particle size of the nanomaterials depending on the type of the material. In the present work, the following techniques have been employed to determine the particle size of the materials prepared, by novel method in present investigation.

Experimental techniques used to determine the particle size of the samples are:

1. X-ray Diffraction.
2. Scanning Electron Microscope (SEM).
3. Transmission Electron Microscope (TEM) and High Resolution Transmission Electron Microscope (HRTEM)
4. Scanning Probe Microscope (SPM).

5.2 POWDER X- RAY DIFFRACTION

From the X-Ray diffraction pattern obtained for the samples the particle size of the crystallites in the sample was determined using Scherrer's formula after applying particle strain corrections using Williamson's Hall analysis. The details of these calculations are as given in Section 4.5.3 of Chapter IV.

5.3 SCANNING ELECTRON MICROSCOPE (SEM)

The Scanning Electron Microscope images of the surface of the sample under measurement by scanning it with a high-energy beam of electrons. SEM gives topographical as well as chemical composition [1]. In SEM, accelerated electrons carry significant amounts of kinetic energy that is dissipated in the sample during the interaction of these electrons with the surface atoms in the sample as a result of which multiple signals are produced. Appropriate signals are collected depending upon the mode of operation of the instrument. Signals produced by SEM are secondary electrons, backscattered electrons (BSE), characteristics X rays, light (cathodoluminescence), specimen current and transmitted electrons. SEM can produce very high-resolution magnified images of a sample surface, revealing details about less than 1 to 5nm in size. SEM micrographs have a large depth of field due to its very narrow electron beam which yields a characteristic three-dimensional appearance useful for understanding the surface structure of a sample. Secondary electrons and backscattered electrons are commonly used for imaging samples.

Since the intensity of the BSE signal is strongly related to the atomic number (Z) of the specimen, BSE images can provide information about the distribution of different elements in the sample.

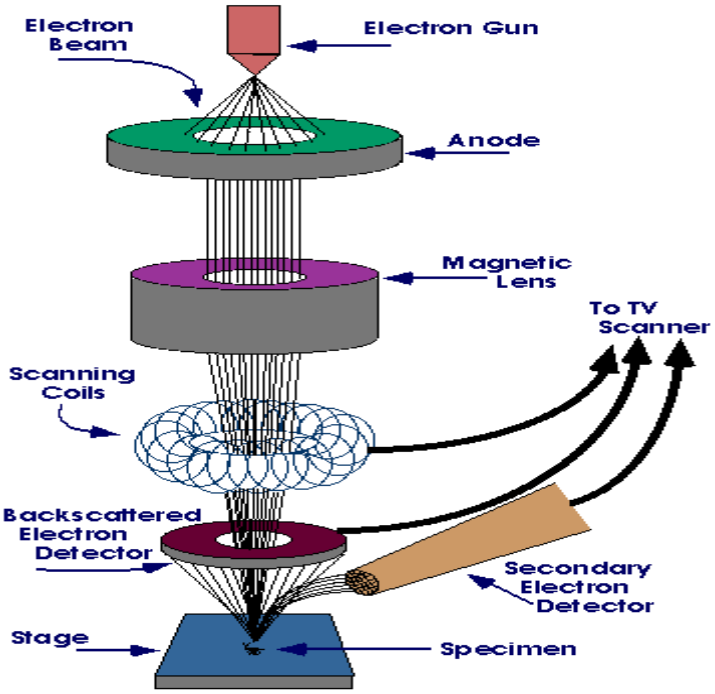

Fig. 5.1(a) Schematic Diagram of Scanning Electron Microscopy (SEM)

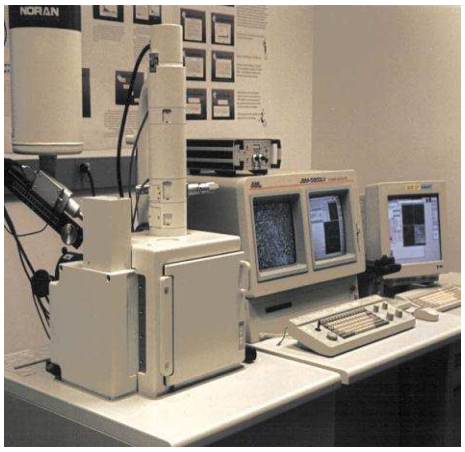

Fig.5.1 (b) : JOEL Model JSM 6360LV (SEM)

Fig. 5. 1 (c) JEOL Model 840 (SEM)

A typical photograph of SEM instrument, showing the electron column, sample chamber, EDS detector, electronics console, and visual display monitor is shown in the fig. 5.1 (b, c)

5.4 TRANSMISSION ELECTRON MICROSCOPY (TEM)

The Transmission Electron Microscope (TEM) has emerged as a powerful tool for probing the structure of metals and alloys. It can give morphological information of shape and size of particles in a microstructure. It can also reveal the nature of crystallographic defects. A detail study of both line defects and planar defects can be carried out in the TEM. Indirect structural information is obtained by making use of the various diffraction techniques available in the TEM. It is capable of yielding composition analysis at nanolevel. With its multifaced capabilities such as nano-beam diffraction and composition analysis and imaging abilities at angstrom level, it has emerged as an instrument for complete characterization of microstructure of materials. TEM's are available in several different forms, which are referred by different acronyms such as HRTEM (High resolution TEM), STEM (Scanning TEM) and ATEM (Analytical TEM).

Fig. 5.2 (a) : TEM Philip model CM 200, electron beam of 200Kev

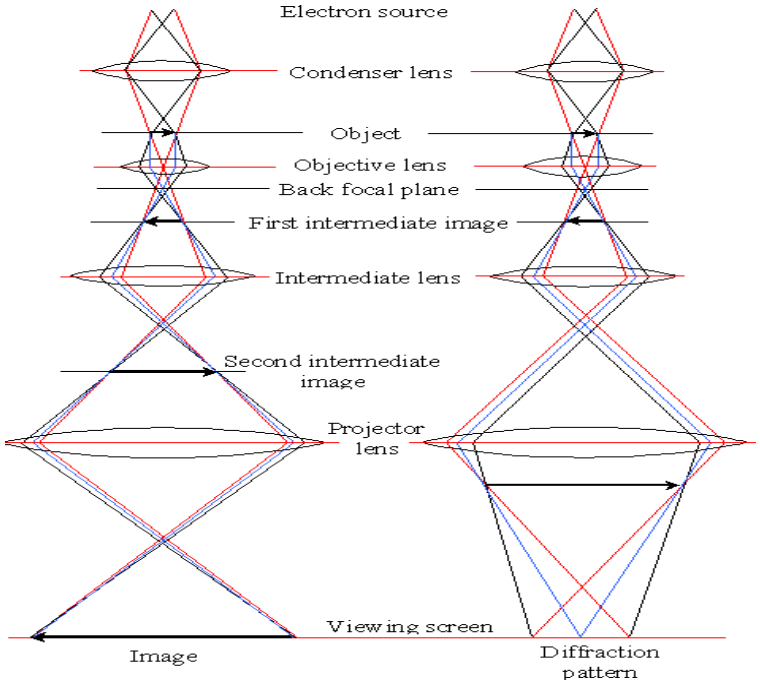

(b) (c)

Figure 5.2 (b,c) The two basic operations of TEM imaging system. (b) Imaging mode and (c) Diffraction pattern

The basic TEM's comprise an electron gun, a vacuum system, electromagnetic lenses, high voltage generator, recording devices and the associated electronics. In order to get the best images, best diffraction effects and the chemical analysis capabilities, the best available electron source needs to be used. The resolution of the modern TEM is under 0.2 nm (point to point) even with a fair amount of specimen tilt. These microscopes are, therefore, capable of resolving the structure of different phases in most metals and alloys.

TEM use low wavelength electron which makes it possible to get a high resolution image. A well focused electron beam obtained from electron gun assembly and electromagnetic condenser lenses is accelerated by an anode, which is typically at +100 keV (in the selective range of 40KeV to 400 keV) with respect to the cathode. The beam is restricted by the condenser aperture, which stops or eliminates un-colliminated electrons. The colliminated high energy (200 Kev and above) beam of electrons strikes the specimen and gets scattered depending upon the thickness and electron transparency of the specimen. Part of the scattered electron beam undergoing phase and amplitude change during scattering is transmitted and the same is focused by the objective lens which forms an image on phosphor screen or charge coupled device (CCD) camera. Adjustable objective apertures can be used to enhance the contrast by blocking out high-angle diffracted electrons.

There are two basic modes of TEM operation: diffraction patterns and imaging modes. As the beam of electrons passes through a crystalline specimen, it is scattered according to the Bragg's law. In order to observe the diffraction pattern, imaging system lenses are adjusted so that the back focal

plane of the objective lens acts as the object plane for the intermediate lens. Then the diffraction pattern is projected onto the viewing screen (Fig.5.2 (c)). While for the imaging mode, the intermediate lens is adjusted so that its object plane is the image plane of the objective lens. The image is then projected onto the viewing screen (Fig 5.2 (b)).

Modern TEM has about five to six image forming lenses. The final image is projected on the screen. The diffraction pattern forms on the back focal plane of the objective lens and the first image forms on the back plane of the objective lens. If the image forming lenses following the objective lens are adjusted in such a way that these see the back focal plane of the objective lens as the object then what one sees on the screen is the diffraction pattern.

However, if the lenses are excited in such a way that these see the back image plane of the objective lens as an object then what we see on the screen is the image of specimen. Therefore, in a modern TEM it is possible to switch from diffraction to imaging and vice-versa by changing the excitation of the lenses following the objective lens. TEM can be used to image the specimen by focusing the final image in the plane of the fluorescent screen or it can be used to image the diffraction pattern from the specimen.

5.4.1. High Resolution Transmission Electron Microscopy (HRTEM)

High-resolution transmission electron microscopy (HRTEM) is an imaging mode of the transmission electron microscope (TEM) that allows the imaging of the crystallographic structure of a sample at an atomic scale [2]. HRTEM can produce images with high resolution below 0.5 Angstrom [3] at magnifications above 50 million times [4]. Because of its high resolution and ability to determine the positions of atoms within materials, it has become a

powerful tool to study nanoscale properties of crystalline materials in nano-technology research and development [5].

The basic working principle of HRTEM is that when a plane wave of electrons is incident on the sample surface, it is attracted by the positive atomic potentials of the atom cores, and channels along the atom columns of the crystallographic lattice. All lattice planes satisfying the Braggs position will diffract the primary beam.The diffraction pattern is the Fourier transform of the periodic potential for the electrons in two dimensions.

In the objective lens, all the diffracted beams and primary beam are brought together and their interference provides a back transformation and leads to enlarged picture of periodic potential. The picture is then magnified by the electron -optical system and finally seen on the screen at a magnefication of around10^6. This imaging process is called phase contrast imaging or high resolution imaging. Due to the inability to record phase of these waves, generally amplitude is measured from these interference pattern. However the phase of the electron wave still carries the information about the sample and generates constrast in the image.

5.5 SCANNING PROBE MICROSCOPE

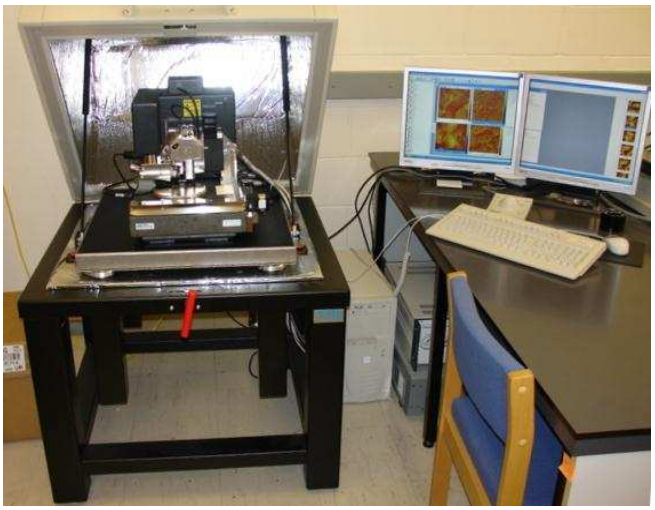

Fig. 5.3 (a) SPM d,I- CALLIBER Model

Scanning probe microscopes (SPM) allows to image, characterize material structures at exceedingly small scales including features of atomic proportions. Scanning probe microscope uses a probe called cantilever that interacts with the sample surface. SPM consist of two major members: Scanning tunneling microscope used for electrically conductive materials, and Atomic Force Microscope for dielectrics.

5.5.2 Scanning tunneling microscope

A Scanning Tunneling Microscope (STM) is an instrument for imaging surfaces at the atomic level. The STM is based on the concept of quantum tunneling. STM can be operated in two modes. In constant current imaging, conductive tip is positioned above the surface of the sample. When the tip moves back and forth across the sample surface at very small intervals, the

height of the tip is contineously adjusted to keep the tunneling current constant. The tip positions are used to construct a topographic map of the surface.

An alternate imaging mode is the constant height operation mode, in which constant height and the bias are simultaneously maintained. As the tip scans the surface, there is a variation in curent due to topographic structure of the sample. Constant current mode produces a contrast directly related to electron charge density profiles of the surface being scanned, whereas the constant height mode permits faster scan rates.

5.5.3 The Atomic Force Microscope

The atomic force microscope (AFM) probes the surface of a sample with a sharp tip, a couple of microns long and often less than 100Å in diameter. The tip is located at the free end of a cantilever that is 100 to 200μm long.

When the tip is brought into proximity of a sample surface, forces between the tip and the sample lead to a deflection of the cantilever. Typically, the deflection is measured using a laser spot reflected from the top surface of the cantilever into an array of photodiodes. Laser light is reflected from the back of the cantilever and is collected by a position sensitive detector (PSD) consisting of two closely spaced photodiodes whose output signal is collected by a differential amplifier. Angular displacement of the cantilever results in one photodiode collecting more light than the other photodiode, producing an output signal which is proportional to the deflection of the cantilever. The measured cantilever deflections allow a computer to generate a map of surface

topography. AFM can be used to study insulators and semiconductors as well as electrical conductors. The primary modes of operation for an AFM are static mode and dynamic mode. In static mode, the cantilever is dragged across the surface of the sample and the contours of the surface are measured directly using the deflection of the cantilever. Static mode AFM is always done in contact where the overall force is repulsive. Consequently, this technique is typically called "contact mode". In contact mode, the force between the tip and the surface is kept constant during scanning by maintaining a constant deflection.

In the dynamic mode or Non-contact mode the cantilever is externally oscillated at or close to its fundamental resonance frequency or a harmonic, where the amplitude of oscillation is typically a few nanometers. The oscillation amplitude, phase and resonance frequency are modified by tip-sample interaction forces. These changes in oscillation with respect to the external reference oscillation allow the scanning software to construct a topographic image of the sample surface.

Dynamic mode operation includes frequency modulation and amplitude modulation. In frequency modulation, changes in the oscillation frequency provide information about tip-sample interactions. In amplitude modulation, changes in the oscillation amplitude or phase provide the feedback signal for imaging. In amplitude modulation, changes in the phase of oscillation can be used to discriminate between different types of materials on the surface. In dynamic contact mode, the cantilever is oscillated such that the

separation distance between the cantilever tip and the sample surface is modulated.

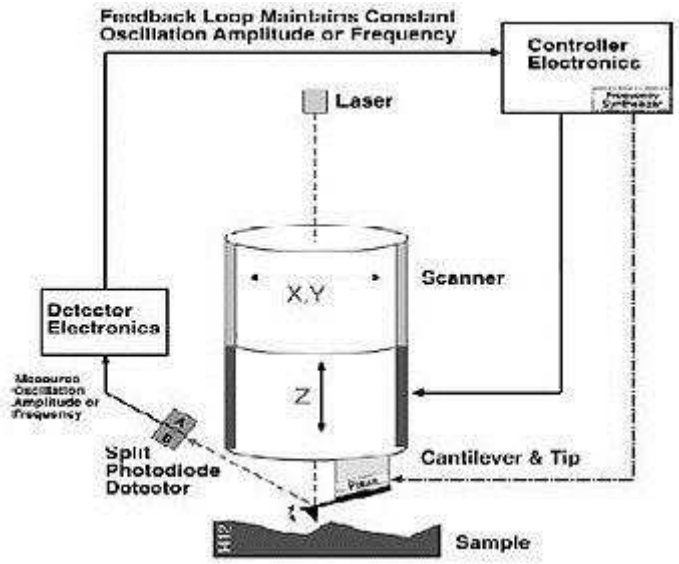

Fig. 5.3 (b) AFM - non-contact mode

AFM has several advantages over the scanning electron microscope (SEM). Unlike the electron microscope, which provides a two-dimensional projection or a two-dimensional image of a sample, the AFM provides a three-dimensional surface profile.

5.6 EXPERIMENTAL

1. XRD Pattern for the powdered samples were obtained on microcomputer controlled Rigaku Diffractometer using Cu K_α(λ=1.5418 Å) from 20^o to 80^o and XRD Desktop miniflex-II (λ=1.5408 Å)

Average particle size estimation was done by substituting XRD peak broadening in Scherrer's formula. Cation distribution, bond length and hopping lengths were calculated using the same.

2. Scanning electron micrograph of powdered sample were obtained on JEOL MODEL 840 and JOEL JSM 6360LV instrument at the accelerating voltage of 10KV

The experimental technique used for determination of SEM micrographs is similar to the one employed for EDS determination, as describe in chapter IV.

3. Transmission electron micrographs are taken on FEI TECNAI 200KV HRTEM and Philip model CM 200 TEM with resolution 0-23nm having an electron beam of 200KeV.

4. Scanning probe micrograph were taken on d- I-CALLIBER SPM and High Resolution Flex AFM

These measurements were carried out to confirm the formation of ultra fine particle size material and to study the surface morphology of sintered samples. Nanoparticles were immobilized on a glass slide on top of a permanent magnet. The particles were imaged by dynamic mode in a High resolution Flax AFM and d, I- CALLIBER SPM.

5.7 RESULTS AND DISCUSSION

5.7.1 Particle Size Estimation

The particle size values obtained for the samples using Scherrer formula after applying Williamson's Hall Plot correction and from TEM are listed in Table 5.1 (a)

Table 5.1 (a): Particle size for nanosamples using XRD and TEM.

Sample	Average particle size 't' (by Williomson Hall Plot) in nm	Average particle size 't' (by using TEM) in nm
$Mn_{0.4}Zn_{0.6}Fe_2O_4$	36.05	30.04(6.43)
$Mn_{0.5}Zn_{0.5}Fe_2O_4$	10.43	10.34(2.20)
$Mn_{0.6}Zn_{0.4}Fe_2O_4$	34.06	39.31(8.44)
$Mn_{0.625}Zn_{0.375}Fe_2O_4$	12.82	11.13(2.17)
$Mn_{0.65}Zn_{0.35}Fe_2O_4$	21.68	8.9(1.71)
$Mn_{0.675}Zn_{0.325}Fe_2O_4$	20.90	13.66(2.69)
$Mn_{0.7}Zn_{0.3}Fe_2O_4$	22.45	15.54(4.06)
$Mn_{0.8}Zn_{0.2}Fe_2O_4$	21.64	21.89(3.86)

5.7.2 Estimation of the Cation Distribution

Spinel ferrite with formula $MeFe_2O_4$ contains two types of sites: tetrahedral site and octahedral sites. The distribution of the cations over these two types of sites can be expressed as [6]

$$Me_{\gamma}\ Fe_{1-\gamma}\ [\ Me_{1-\gamma}\ Fe_{1+\gamma}]\ O_4$$

where the square bracket include the ions at the octahedral sites, and γ is a constant which can determine the cation distribution. For the system under investigation $Mn_xZn_{1-x}Fe_2O_4$, the cation distribution can be expressed as

$$Zn_{\delta}\ Mn_{\gamma}\ Fe_{1-\gamma-\delta}\ [\ Zn_{1-x-\delta}\ Mn_{x-\gamma}\ Fe_{1+\gamma+\delta}\ ]\ O_4$$

Therefore, the mean radius of the ion at the tetrahedral site is given by

$$r_{tetr} = \delta\ r_{Zn} + \gamma\, r_{Mn} + (1-\gamma-\delta)\, r_{Fe}$$

and the mean radius of the ion at the octahedral site is given by

$$r_{oct.} = \frac{1}{2}[\ (1-x-\delta) r_{Zn} + (x-\gamma)\, r_{Mn} + (1+\gamma+\delta)\, r_{Fe}\ ]$$

From the other hand also, the mean radius of the ions at tetrahedral site and octahedral site is given by [**7]**

$$r_{tetr.} = a\sqrt{3}\ (u - 0.25) - R_o$$

$$r_{oct.} = a\ (\frac{5}{8} - u) - R_o$$

where R_o is the radius of the oxygen ion (1.26 Å) and u is the oxygen parameter. Solving above Eqns. both δ and γ can be determined. Table (5.1 (b)) shows the estimated cation distribution for these samples.

Table 5.1 (b): Estimated cation distribution for $Mn_xZn_{(1-x)}Fe_2O_4$ using X-ray results.

Sample	Tetrahedral Site	Octahedral Site
$Mn_{0.4}Zn_{0.6}Fe_2O_4$	Mn(0.363)Zn(0.114)Fe(0.523)	Mn(0.037)Zn(0.486)Fe(1.477)
$Mn_{0.5}Zn_{0.5}Fe_2O_4$	Mn(0.358)Zn(0.126)Fe(0.517)	Mn(0.142)Zn(0.374)Fe(1.483)
$Mn_{0.6}Zn_{0.4}Fe_2O_4$	Mn(0.359)Zn(0.147)Fe(0.494)	Mn(0.241)Zn(0.253)Fe(1.506)
$Mn_{0.625}Zn_{0.375}Fe_2O_4$	Mn(0.360)Zn(0.153)Fe(0.487)	Mn(0.265)Zn(0.222)Fe(1.513)
$Mn_{0.65}Zn_{0.35}Fe_2O_4$	Mn(0.362)Zn(0.163)Fe(0.475)	Mn(0.288)Zn(0.187)Fe(1.525)
$Mn_{0.675}Zn_{0.325}Fe_2O_4$	Mn(0.366)Zn(0.183)Fe(0.452)	Mn(0.309)Zn(0.142)Fe(1.548)
$Mn_{0.7}Zn_{0.3}Fe_2O_4$	Mn(0.366)Zn(0.181)Fe(0.454)	Mn(0.334)Zn(0.119)Fe(1.546)
$Mn_{0.8}Zn_{0.2}Fe_2O_4$	Mn(0.362)Zn(0.192)Fe(0.446)	Mn(0.438)Zn(0.008)Fe(1.554)

5.7.3 The Interionic Distances

The interionic distances *(i.e.* cation–anion distances at A-site, d_{AL}, and B-site, d_{BL}, together with the distance of closest anion–anion approach, tetrahedral edge, d_{AE}, and shared and unshared octahedral edges, d_{BE}, d_{BEU}) are calculated according to the following Eqns. [8]:

$$d_{AL} = a\ \sqrt{3}\left(u - 0.25\right)$$

$$d_{BL} = a\left(3u^2 - \frac{11}{4}u + \frac{43}{64}\right)^{1/2}$$

$$d_{AE} = a\sqrt{2}\left(2u - 0.5\right)$$

$$d_{BE} = a\sqrt{2}\left(1 - 2u\right)$$

$$d_{BEU} = a\left(4u^2 - 3u + \frac{11}{16}\right)^{1/2}$$

The obtained values are listed in Table 5.1 (c)**.** It is clear that the values of d_{AL}, d_{BL}, d_{AE}, d_{BE}, and d_{BEU} increase with increasing Mn ion content. This variation may be attributed to the substitution process and the cation distribution.

The distance L_A and L_B between the magnetic ions at A–site and B–site respectively can be obtained, where, $L_A = a\sqrt{3}/4$**,** and $L_B = a\sqrt{2}/4$ [9]. The obtained values of L_A and L_B are listed in Table 5.1 (c) Maximum value of L_A is 3.666A^o for the sample $Mn_{0.8}Zn_{0.2}Fe_2O_4$ and minimum value of L_A is 3.648 A^o for the sample $Mn_{0.4}Zn_{0.6}Fe_2O_4$ at A-site. Maximum value of L_B is 2.993

Å and minimum value is 2.978 Å at B- site for the samples $Mn_{0.8}Zn_{0.2}Fe_2O_4$ and the sample $Mn_{0.4}Zn_{0.6}Fe_2O_4$ respectively.

Table 5.1 (c): The bond length of A-sites d_{AL} and B-sites d_{BL}, the tetrahedral edge d_{AE}, the shared and unshared octahedral edges, d_{BE} and d_{BEU}, and the hopping length at A-site L_A and at B-site L_B for each sample.

Sample	d_{AL} Å	d_{BL} Å	d_{AE} Å	d_{BE} Å	d_{BEU} Å	L_A Å	L_B Å
$Mn_{0.4}Zn_{0.6}Fe_2O_4$	1.824	2.106	2.978	2.978	2.978	3.648	2.978
$Mn_{0.5}Zn_{0.5}Fe_2O_4$	1.825	2.107	2.979	2.979	2.979	3.649	2.979
$Mn_{0.6}Zn_{0.4}Fe_2O_4$	1.827	2.110	2.983	2.983	2.983	3.654	2.983
$Mn_{0.625}Zn_{0.375}Fe_2O_4$	1.828	2.111	2.985	2.985	2.985	3.656	2.985
$Mn_{0.65}Zn_{0.35}Fe_2O_4$	1.829	2.113	2.987	2.987	2.987	3.659	2.987
$Mn_{0.675}Zn_{0.325}Fe_2O_4$	1.831	2.114	2.990	2.990	2.990	3.663	2.990
$Mn_{0.7}Zn_{0.3}Fe_2O_4$	1.832	2.115	2.991	2.991	2.991	3.665	2.991
$Mn_{0.8}Zn_{0.2}Fe_2O_4$	1.833	2.116	2.993	2.993	2.993	3.666	2.993

5.7.4 SEM Micrograph

SEM Micrograph of nanosamples:

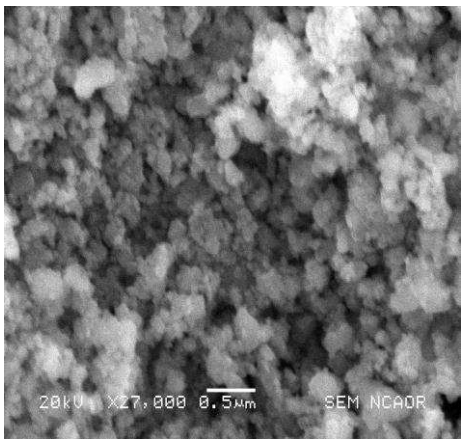

5.4 (a): SEM Micrograph of $Mn_{0.675}Zn_{0.375}Fe_2O_4$

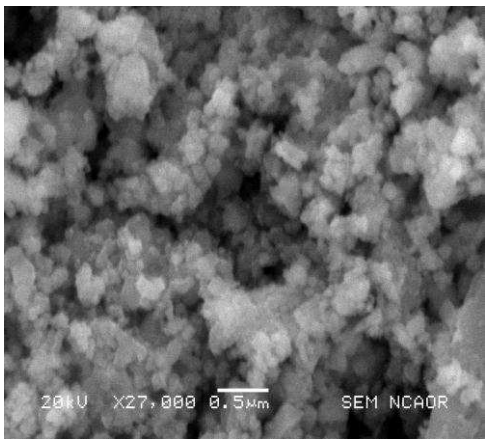

5.4 (b) SEM Micrograph of $Mn_{0.6}Zn_{0.4}Fe_2O_4$

SEM image of nanosamples is not well resolved, because samples are highly magnetic and intensity of electron beam of SEM may not be sufficient to provide the required resolution to make estimates of nanoparticle sizes. Thus the particles are not well resolved and magnified. This fact makes it impossible to make accurate estimates of particle size distribution of SEM image of nanosamples.

SEM Micrographs of sintered samples and the particle size histograms of the same are given in the corresponding figures below:

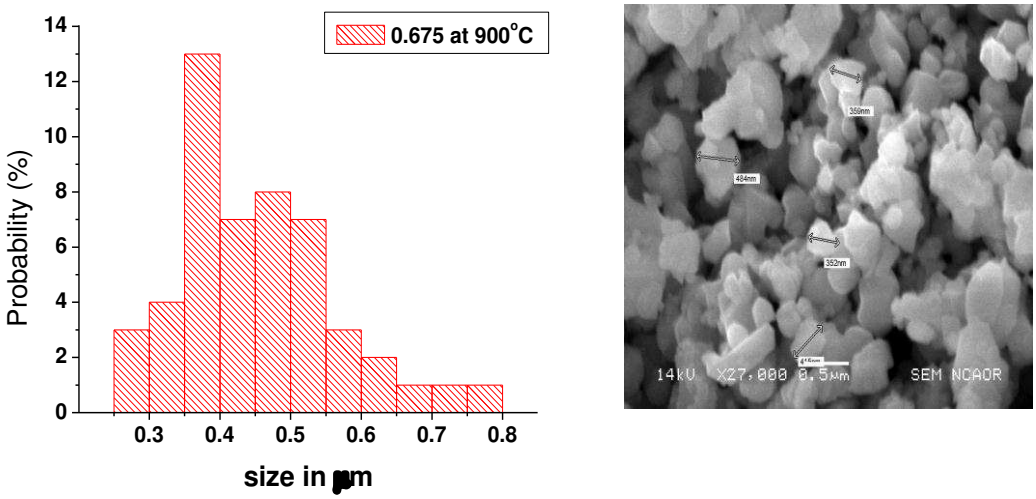

Fig.5.4 (c) SEM Micrograph of bulk sample $Mn_{0.675}Zn_{0.325}Fe_2O_4$ (900°C)

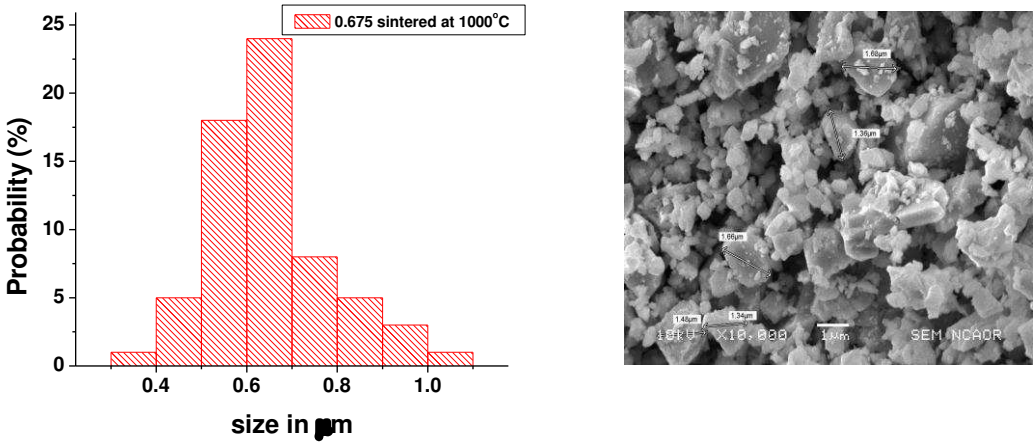

Fig.5.4 (d) SEM Micrograph of bulk sample $Mn_{0.675}Zn_{0.325}Fe_2O_4$ (1000°C)

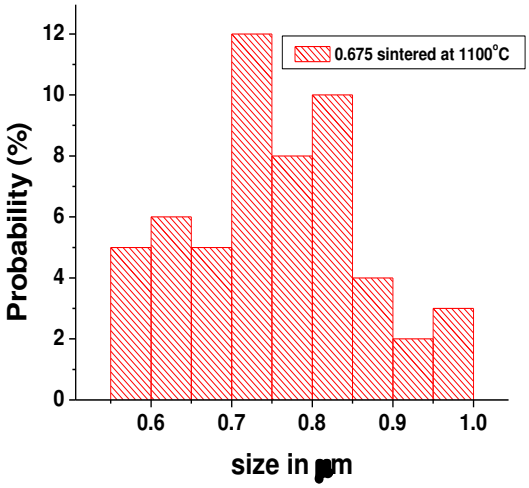

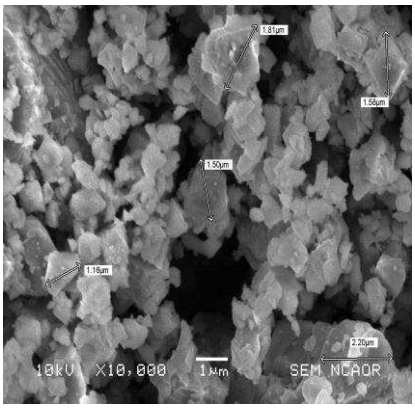

Fig.5.4 (e) SEM Micrograph of bulk sample $Mn_{0.675}Zn_{0.325}Fe_2O_4$ (1100°C)

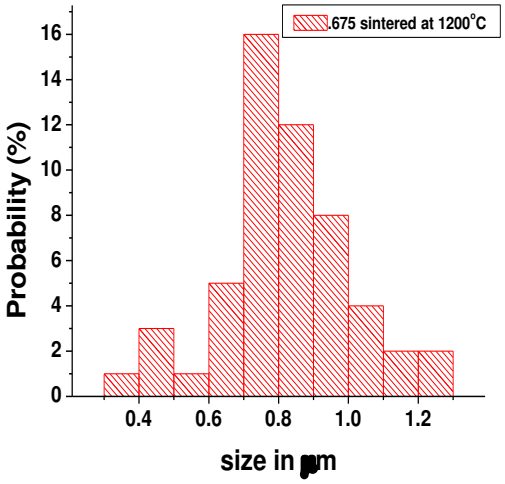

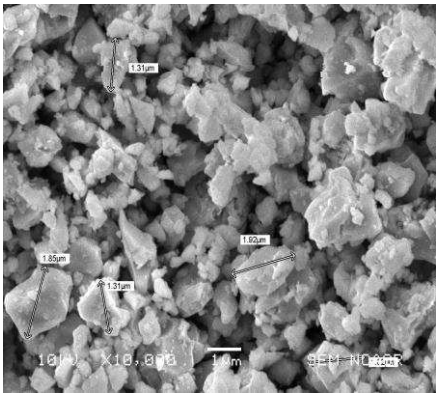

Fig.5.4 (f) SEM Micrograph of bulk sample $Mn_{0.675}Zn_{0.325}Fe_2O_4$ (1200°C)

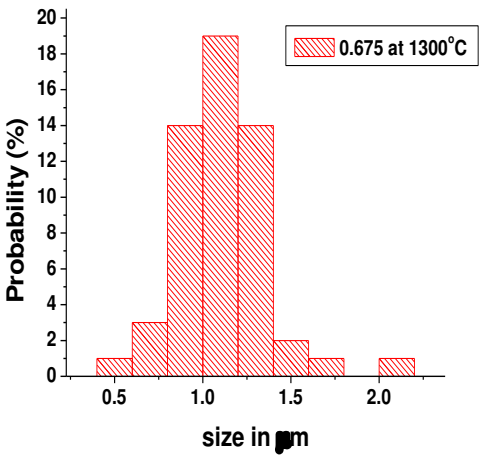

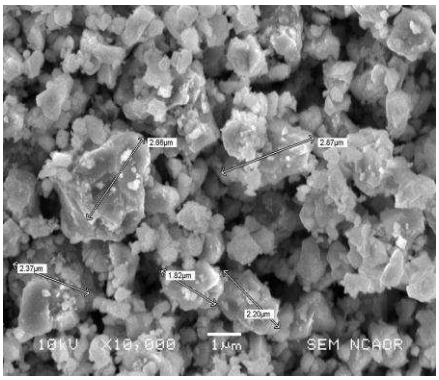

Fig.5.4 (g) SEM Micrograph of bulk sample $Mn_{0.675}Zn_{0.325}Fe_2O_4$ (1300°C)

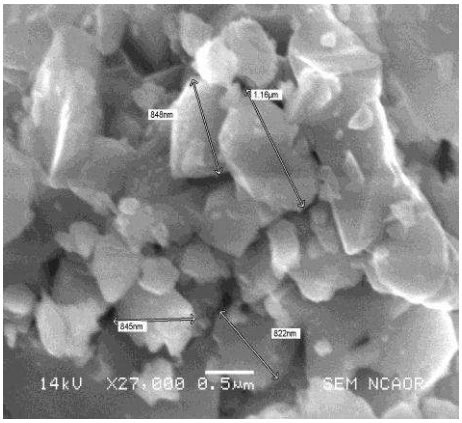

Fig. 5.4(h) bulk sample $Mn_{0.6}Zn_{0.4}Fe_2O_4$ (1100^oC)

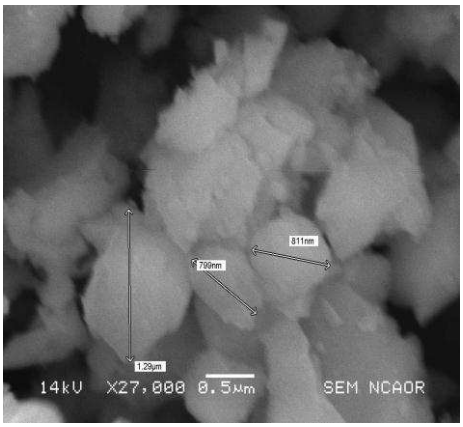

Fig. 5.4(i) bulk sample$Mn_{0.6}Zn_{0.4}Fe_2O_4$ (1300^oC)

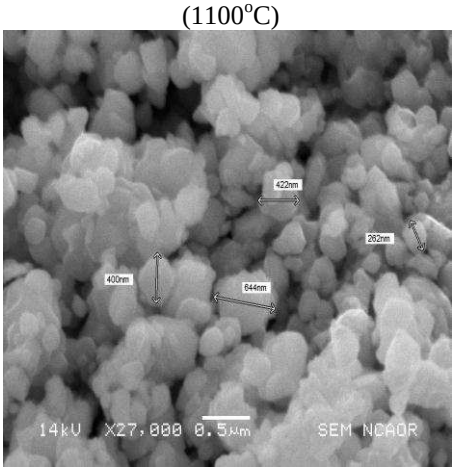

Fig. 5.4(j) bulk sample $Mn_{0.625}Zn_{0.375}Fe_2O_4$ (1000^0C)

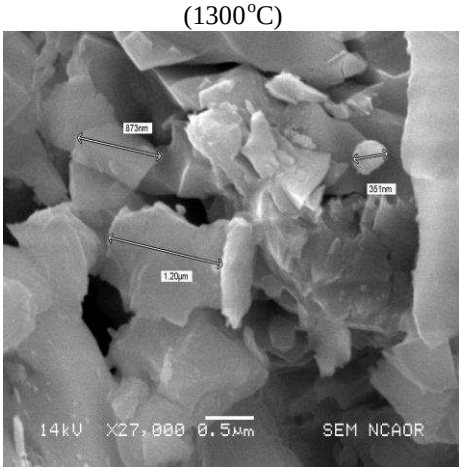

Fig. 5.4(k) bulk sample $Mn_{0.625}Zn_{0.375}Fe_2O_4$ (1200^0C)

Fig. 5.4 (h,i) SEM micrograph of bulk sample $Mn_{0.6}Zn_{0.4}Fe_2O_4$ (1100^0C, 1300^0C) and 5.4 (j.k) SEM micrograph of bulk sample $Mn_{0.625}Zn_{0.375}Fe_2O_4$ (1000^0C, 1200^0C)

Particle size of fifty individual particles was determined using image J software to obtain the histogram for particle size distribution. The histogram of bulk sample $Mn_{0.675}Zn_{0.35}Fe_2O_4$ obtained at 900^oC shows that the maximum size distribution is in the range of 0.35µm to 0.55µm. At 1000^oC, maximum size distribution is in the range of 0.5µm to 0.7µm, which increases to 0.7 µm to 0.9µm at 1200 ^oC, whereas for the same sample sintered at 1300^oC, the

maximum size distribution is in the range of 0.75µm to 1.5µm. These results indicate that particle size of bulk samples increase with increase in sintering temperature as expected.

5.8 TEM Micrograph

Fig. 5.5 (a, b, c, d, e, f) are the TEM Micrographs of samples and the corresponding histograms for particle size.

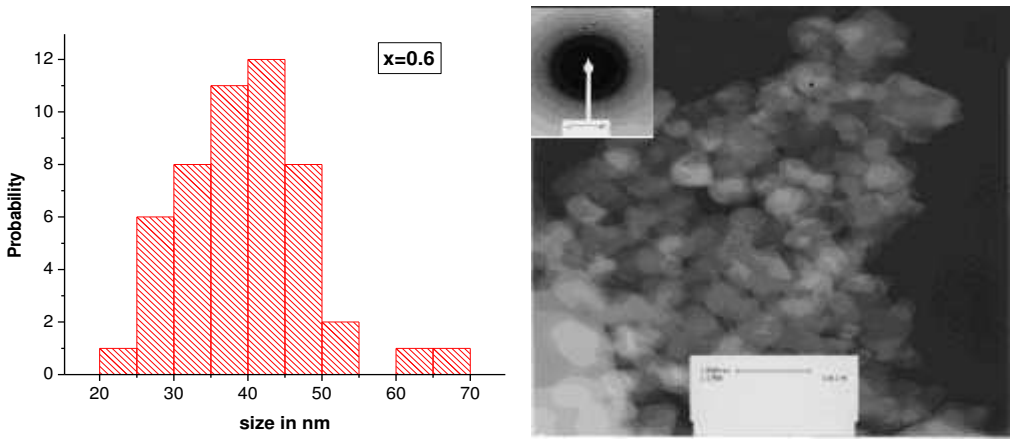

Fig.5. 5 (a) TEM micrograph & Histogram of $Mn_{0.6}Zn_{0.4}Fe_2O_4$

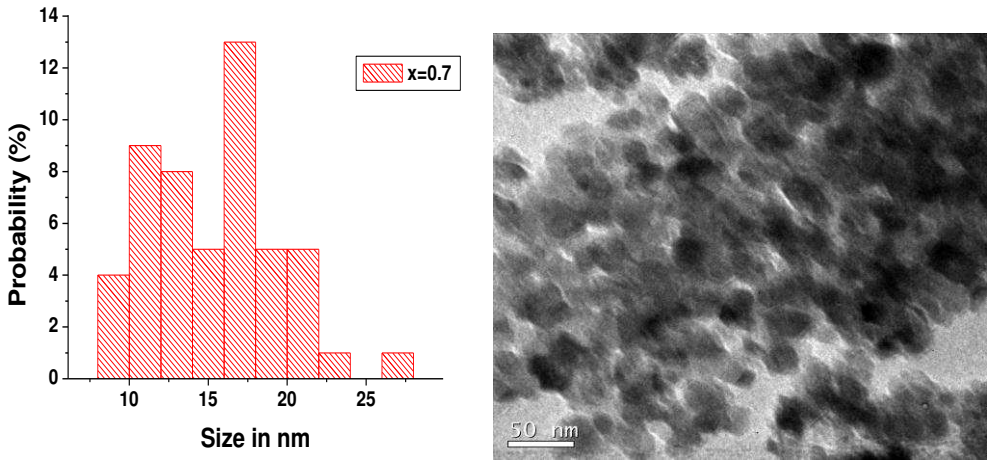

Fig.5.5 (b) TEM micrograph & Histogram of $Mn_{0.7}Zn_{0.3}Fe_2O_4$

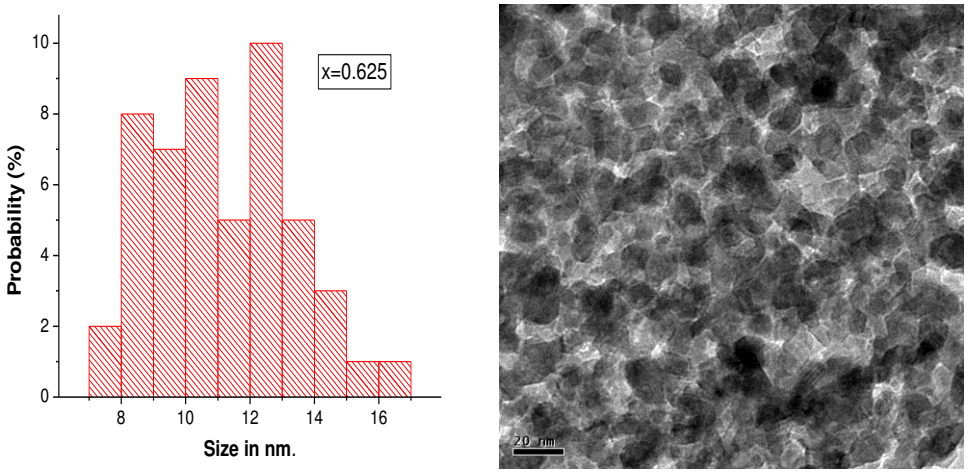

Fig.5.5 (c) HRTEM Micrograph and Histogram of $Mn_{0.625}Zn_{0.375}Fe_2O_4$

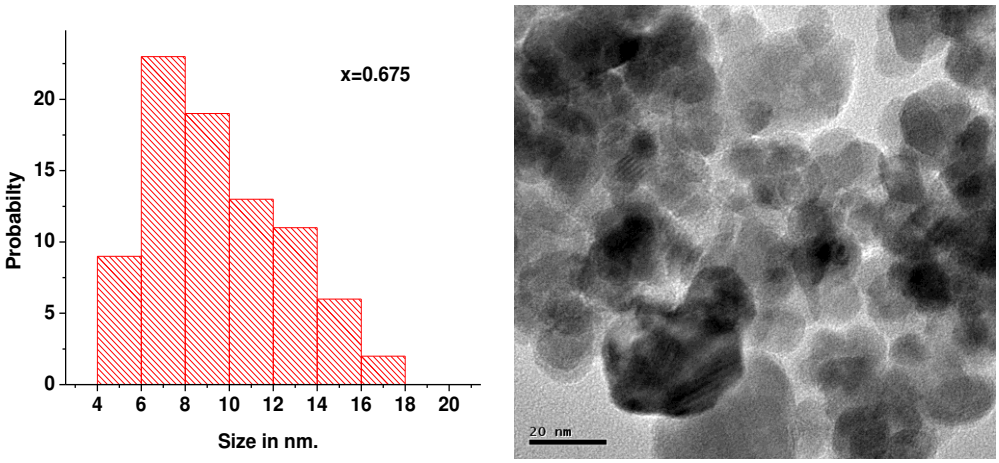

Fig. 5.5 (d) HRTEM Micrograph and Histogram of $Mn_{0.675}Zn_{0.0.325}Fe_2O_4$

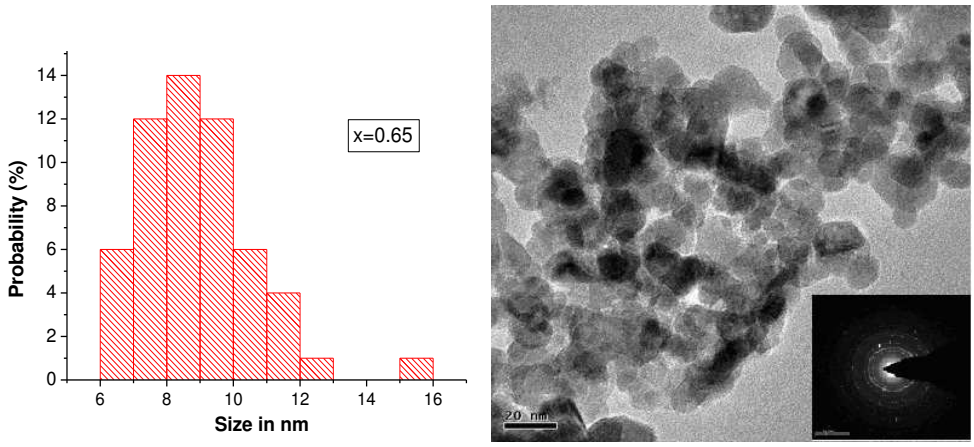

Fig.5. 5 (e) HRTEM micrograph and Particle Size Histogram of $Mn_{0.65}Zn_{0.35}Fe_2O_4$

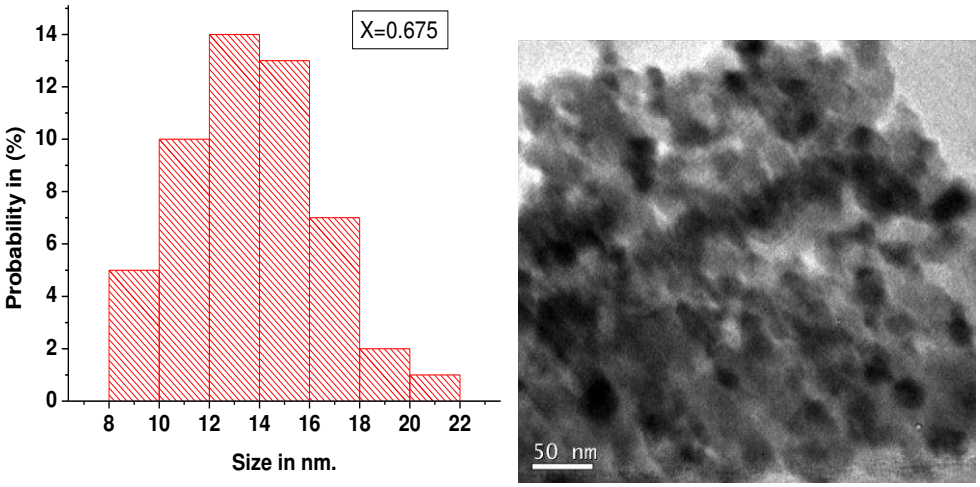

Fig.5. 5 (f) HRTEM Micrograph and Histogram of $Mn_{0.675}Zn_{0.0.325}Fe_2O_4$

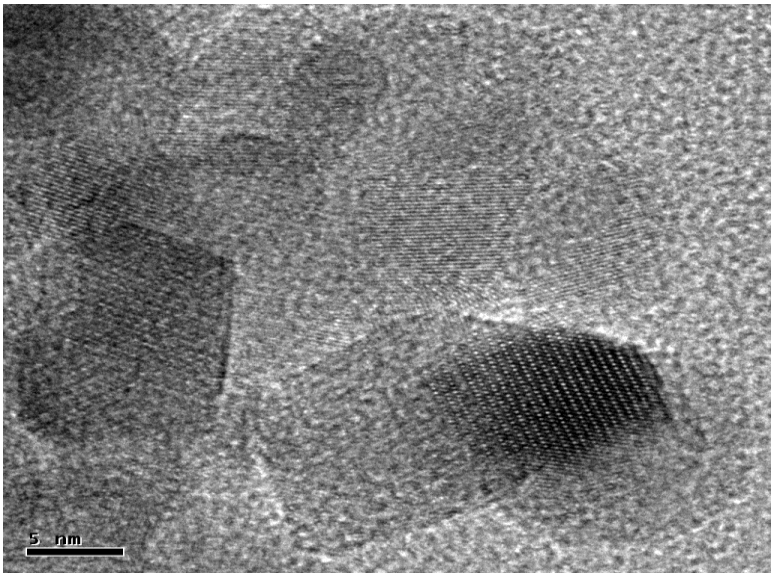

Fig.5.6 (a) HRTEM micrograph $Mn_{0.65}Zn_{0.35}Fe_2O_4$

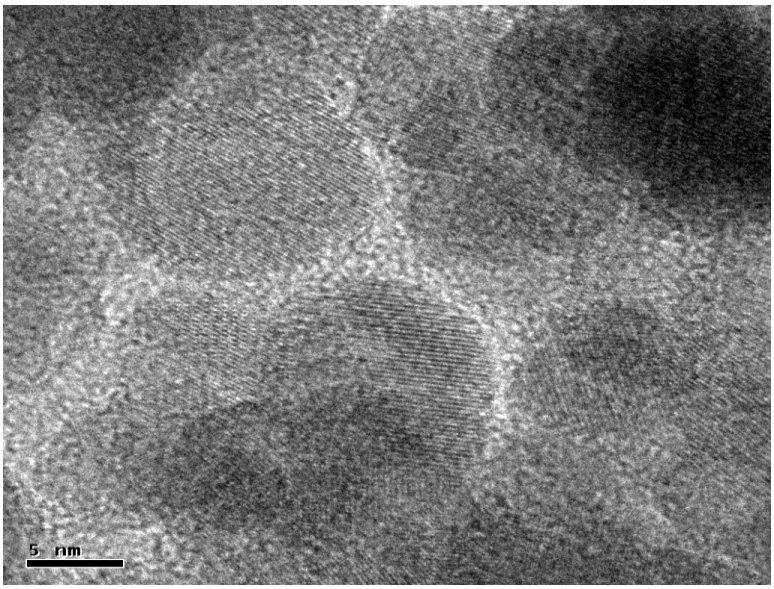

Fig. 5.6 (b) HRTEM micrograph $Mn_{0.65}Zn_{0.35}Fe_2O_4$

The average size of nanoparticles calculated from the peak broadening, and after applying Williamsons Hall Plot correction for particle strain broadening in the x-ray diffraction pattern by using Scherrer formula [10], gives an overall particle size for the samples in the range of 10 nm to 36 nm. However the average particle size of the same samples seen from TEM and

HRTEM is in the range of 8 to 40 nm. This is in good agreement with the particle size estimated from Scherrer formula.

Transmission electron microscopy (TEM) and High Resolution microscopy have been used to confirm the nanoparticle size and to determine the particle size distribution. The size distribution has been determined from the histogram obtained by measuring the size of around sixty individual particles using image J software. The histogram of sample $Mn_{0.60}Zn_{0.40}Fe_2O_4$, shows that the maximum size distribution is in the range of 35nm to 45nm, for the sample $Mn_{0.7}Zn_{0.3}Fe_2O_4$, it is in the range of 16nm to 18nm, for the sample $Mn_{0.625}Zn_{0.375}Fe_2O_4$ it is in the range of 8nm to 13nm, and for the sample $Mn_{0.65}Zn_{0.35}Fe_2O_4$, it is in the range of 7nm to 10nm.The high resolution TEM image of $Mn_{0.65}Zn_{0.35}Fe_2O_4$, shows clearly the lattice fringes of these nanocrystallites (Fig.5.6 (a) & 5.6 (b)).

5.9 Scanning Probe Microscope

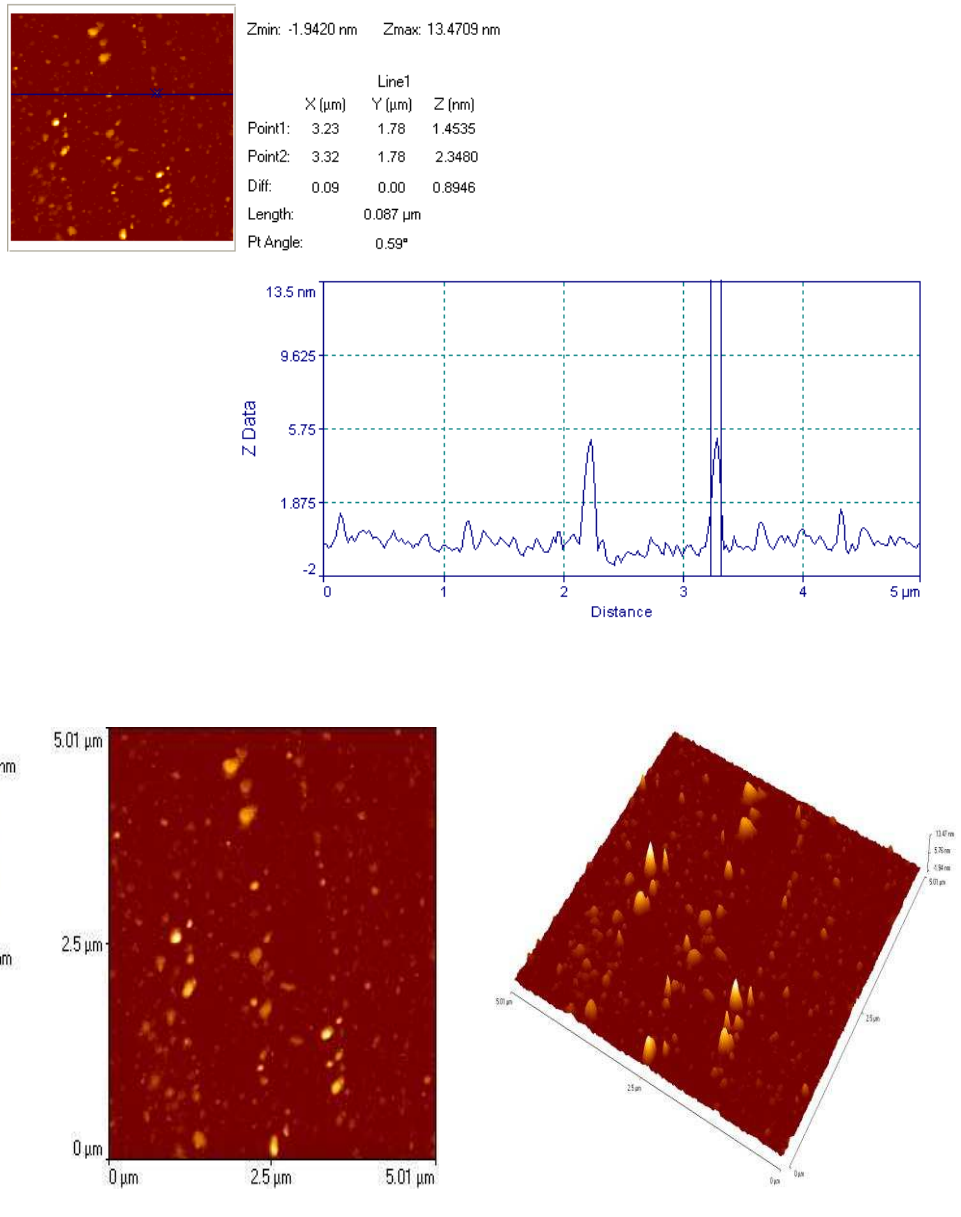

5.7 SPM Micrograph of nanosample $Mn_{0.6}Zn_{0.4}Fe_2O_4$

SPM Micrograph of nanosample $Mn_{0.6}Zn_{0.4}Fe_2O_4$ provides three dimensionional information of the particle size (Fig.5.7). Particle size analysis carried out on SPM micrographs indicates formation of polycrystalline fine grain material with one dimension in nanometer. Particles of different sizes are visible in the Fig.5.7.

In conclusion, the particle size analyses carried with the help of the XRD and the most modern microscopy tools like TEM, HRTEM, and SPM, show that all the samples under investigation, prepared using the new preparative technique are nanoparticle, and some of the samples have a narrow range of particle size distribution. Thus, the new method developed can be used as a potential method for production of nanoparticle Mn-Zn ferrite materials.

References

[1] Guozhonq Cao, Nanostructures and Nanomaterials, synthesis, Properties and Applications, publication 2004, Reprinted 2005, 2006, Imperial college press.

[2] R. W. Cahn, P. Haasen, E. J. Kramer, Material Science and Technology Vol.2A, VCH-Weinheim-Newyork.

[3] R. W. Cahn, P. Haasen, E. J. Kramer, Material Science and technology Vol.2B, VCH-Weinheim-Newyork.

[4] P. J. Goodhew and F. J. Humhreys, Taylor and Francis, Electron Microscopy and Analysis, London ,(1988).

[5] D. B. Williams and C. B. Carter, Transmission Electron Microscopy, Plenum Press, Newyork, (1996).

[6] A. A. Yousif, M. E. Elzain, S. A. Mazen, H. H. Sutherland, M. H. Abdalla, and S. F. Mansour, J. Phys. Condens. Matter **6**, 5717 (1994).

[7] J. Smit and H. P. J. Wijn, "Ferrites", Cleaver-Hume. Press, London, (1959).

[8] C. Otero Arean, E. Garcia Diaz, J. M. Rubio Gonzalez and M. A. Villa Garcia, J. Sol. State Chem. **77** (1988) 275.

[9] B. Gillot and F. Jemmali, phys. stat. sol. (a) **76** (1983) 601.

[10] B. D. Cullity, Elements of X-ray Diffraction, 2nd edition, Addison Weseley (1978).